THE GIANT BRANCH OF LEO I

by

MICHAEL FRANZ FOX

B.Sc., University of Newcastle upon Tyne, 1985

A THESIS SUBMITTED IN PARTIAL FULFILLMENT

OF THE REQUIREMENTS FOR THE DEGREE OF

MASTER OF SCIENCE

in the Department

of

Physics

ACCEPTED

FACULTY OF GRADUATE STUDIES

[redacted]

DEAN

DATE Sept 8, 1987

We accept this thesis as conforming

to the required standard

[redacted]

C. J. Pritchet

[redacted]

D. A. VandenBerg

[redacted]

V. Tunnicliffe

[redacted]

P.B. Stetson

Supervisor: Professor Christopher J. Pritchet

ABSTRACT.

A colour-magnitude diagram down to V=22 is presented for the dwarf spheroidal galaxy Leo I. The morphology of the colour-magnitude diagram is found to be strikingly similar to that of Leo II and Fornax. A prominent, wide giant branch is visible, indicating a spread in metallicity of nearly 1.0 dex, with a mean around [Fe/H]=-1.4. The traditional distance modulus of (m-M)=21.8 is confirmed. Known carbon stars are found to lie at or above the tip of the first giant branch. An asymptotic giant branch is also seen, but the horizontal branch (presumably at V~22.5) is fainter than the limit of the data.

Examiners:

[redacted]

C. J. Pritchet

[redacted]

D. A. VandenBerg

[redacted]

V. Tunnicliffe

[redacted]

P.B. Stetson

Table of Contents

List of Tables

List of Figures

Glossary

AGB — Asymptotic Giant Branch. Locus in the colour-magnitude diagram where post-HB stars are found. These stars have an isothermal carbon-oxygen core, and are burning hydrogen and helium in shells. The track asymptotically approaches the giant branch.

B — The standard Johnson 'B' filter (λλ 3900-4900), or the magnitude of an object through this filter.

Carbon star — A star whose atmospheric abundance of carbon is greater than that of oxygen, and whose spectrum hence shows unusually strong carbon features.

Colour — The difference in magnitude of an object through two different filters.

Dex — Unit of [Fe/H].

Distance modulus — (m-M) This distance measure is the difference between the apparent (observed) magnitude of an object and its absolute magnitude, which is the magnitude it would have at a distance of 10 parsecs.

[Fe/H] — A logarithmic measure of metallicity, expressed as the number abundance ratio of Fe to H, relative to solar values.

Field star — A star that lies in the same direction as the cluster under investigation, but is not a member of the cluster (usually foreground objects).

GC	Globular Cluster. A compact, spherical conglomeration of typically 10^5-10^6 stars. These systems tend to be found in a spherically symmetric distribution around the centers of larger galaxies.
Giant branch	Locus in the colour-magnitude diagram where the red giant stars are found. These stars have an isothermal helium core, with energy generation by hydrogen burning in a thin shell.
HB	Horizontal Branch. Locus in the colour-magnitude diagram where are found stars burning helium in the core.
Magnitude	A logarithmic scale of brightness.
Metallicity	The metal content of a star or galaxy. All elements other than hydrogen and helium are considered to be metals.
PSF	Point-Spread Function. A three dimensional function that describes the shape of the instrumental response to the light from a point source. The PSF varies from one exposure to the next.
Reddening	The absorption of light caused by interstellar dust that tends to make colours redder.
V	The standard Johnson 'V' filter ($\lambda\lambda$ 5100-5900), or the magnitude of an object through this filter.

Acknowledgements

The author would like to thank C. J. Pritchet for his continued support and encouragement throughout the course of this research. Both C. J. Pritchet and D. A. VandenBerg provided constructive criticism and much needed advice which has significantly improved the quality of this thesis. Thanks are also due to L. Infante for assistance with the observations.

Finally, the author would like to express his gratitude to the University of Victoria for financial support in the form of a Graduate Fellowship.

Voor Moeder, wiens volharding in een moeilijke begintijd

nu de moeite waard blijkt te zijn.

1. INTRODUCTION

The Object

The Leo I galaxy is a member of the Local Group of Galaxies, and is apparently associated with the Milky Way. It was discovered by Harrington and Wilson (1950) on the Palomar Observatory Sky Survey plates. Although just close enough to the Sun to be resolved into individual stars, it is still far enough away to be very faint, making observation rather difficult. On the basis of its appearance it has been classified as a dwarf spheroidal galaxy, of which there are seven known surrounding the Milky Way. These galaxies are so small and faint that very few are known at greater distances.

Although dwarf spheroidals have the general appearance of elliptical galaxies on a photographic plate, studies of their dynamic and photometric properties suggest they are intrinsically a different kind of object altogether. Not only in size, but in many other ways do they seem to be intermediate between real galaxies and the globular clusters normally found around large galaxies. On the other hand they show a number of peculiarities that astronomers have as yet been unable to explain. One example of these is the way dwarf spheroidals tend to show a red horizontal branch in the colour-magnitude diagram even though they are metal-poor. With globular clusters, only metal-rich clusters show a red horizontal branch.

The Colour-Magnitude Diagram

The colour-magnitude diagram is an observational version of the Hertzsprung-Russell diagram, where stars are plotted with effective temperature on the horizontal axis and absolute luminosity on the vertical. This diagram can be used to classify stars, as stars in different stages of their life appear in different parts of the diagram. Both of the quantities used to plot the Hertzsprung-Russell diagram are difficult to obtain in practice however. Fortunately, it was found that a very similar diagram could be constructed using just the observational magnitudes V and B. The V magnitude scales directly with the absolute luminosity, provided the distance effect is removed, and is hence used for the vertical axis. A colour index is formed as (B-V), which turns out to be an indicator of the effective temperature. This is plotted on the horizontal axis.

When the stars in a cluster are plotted in such a colour-magnitude diagram, they fall on certain principal sequences. Most stars are in the stable hydrogen-burning phase of their life, and lie on the main sequence. Some however, are older and more evolved; these are in the red giant phase, and lie on the giant branch in the diagram. Still others are in a quasi-stable helium-burning phase, and appear on the horizontal branch. The exact shapes and positions of the principal sequences contain information about the cluster, e.g. its distance and metal content. Because of the comparative ease with which such a diagram can usually be obtained, it is therefore one of the first things normally done for a new cluster.

The Instrument

The instrument used to detect and record the image of the galaxy is known as a Charge Coupled Device (CCD). At the heart of the device is a photosensitive silicon chip, divided into rows and columns of picture elements (pixels, in this case 320 by 512). When a photon strikes the surface of the chip, an electron-hole pair is created. The positive hole drifts away and the electron is trapped in the nearest pixel by means of an electric potential that is applied to each element. The intensity of light falling onto each pixel is therefore directly proportional to the charge accumulated in the pixel. On termination of the exposure, this charge can be read out and stored in a computer or on a magnetic tape. The CCD therefore produces an image which looks very much like a conventional photograph when displayed on a TV screen. CCD images, however, have a number of advantages which facilitate the reduction process and allow a greater precision of measurement to be achieved.

First of all, the mere fact that the data is in digital form avoids the need to digitize. It can be conveniently handled and analysed by numerical techniques on a computer in its original form. Secondly the sensitivity of the silicon chip is much higher than that of photographic plates. This means fainter objects can be detected in less time. Finally the response of the CCD is linear over a wide range in magnitude whereas photographic emulsions have neither a linear response nor a wide dynamic range.

Along with these advantages, there are two main drawbacks inherent in the present day CCD. The sensitivity of silicon diminishes rapidly in the infrared, where the energy of the photons drops below the threshold energy for electron-hole pair creation. Therefore a CCD is not suited to work that involves longer wavelengths. The other is a technological difficulty. The largest CCDs currently available are approximately 1000 pixels square; it proves difficult to manufacture larger chips of good quality. The physical size of the light sensitive area is then approximately one square centimeter, whereas photographic plates can be tens of centimeters across. At the telescope this means that the field of view accessible to a CCD is very small compared to that of a photographic plate. For some work, e.g. surveys, a large field of view is essential, thereby eliminating CCDs as a useful detector. For the present study, neither of these points presents a problem.

Previous Work

Leo I is located at an angular distance of only 20 arcmin from Regulus, one of the brightest stars in the sky. Consequently it is a very difficult object to observe. Photographic work with large reflectors is virtually impossible, as ghost images and other scattered light from Regulus invariably cause the galaxy to be contaminated. In fact, Leo I is the only one of the seven known dwarf spheroidal systems associated with our Galaxy without a colour-magnitude diagram (CMD).

As a result of these observational difficulties, little optical work has been done on Leo I. Hodge and Wright (1978) surveyed the

galaxy for variable stars and found 23 variables, mainly anomalous Cepheids and RR Lyrae stars. Furthermore, Hodge and Wright found the distance modulus to be (m-M)=21.7 from the brightest member giants. From a rough CMD produced by measuring the brightest stars on their plates, they noted the existence of a conspicuous giant branch, reaching V=20 at (B-V)=1.4. This result is in agreement with the present data (see Chapter 4). (See also Fig. 4.3 of Hodge 1986.)

Azzopardi, Lequeux and Westerlund (1985, henceforth ALW) have discovered 13 certain and 4 possible carbon stars in Leo I. This number includes 1 star originally found by Aaronson, Olszewski and Hodge (1983). As in the other dwarf spheroidal galaxies, the carbon stars are among the brightest members of Leo I, implying the existence of a "young" ($<10^{10}$ y old) stellar population. Nevertheless, no star formation can be occurring at the present time, since Knapp et al. (1978) have placed stringent upper limits on the H I content of Leo I.

Suntzeff et al. (1986) reported spectroscopy of 2 giants in Leo I, yielding an estimate of the metal abundance [Fe/H]=-1.5 ± 0.25. This is the first reliable indicator of the chemical composition of this system, and employing this metallicity estimate Leo I fits very well onto the luminosity-metallicity correlation for dwarf spheroidal galaxies (Aaronson and Mould 1985, Zinn 1985). With only 2 stars measured, with relatively large errors, it is impossible to approach the question of a spread in metallicity.

CMD's reaching the main sequence turnoff are available for the five closer dwarf spheroidals. Comparison of these CMD's shows a large

variation in metallicity from galaxy to galaxy, although none is metal-rich. In all cases the giant branch is significantly wider than seen in globular clusters. The most plausible explanation for this result is an intrinsic variation in metallicity from star to star in each of the galaxies, a theory that is increasingly supported by spectroscopic evidence.

To obtain a preliminary CMD of Leo I, imagery of this galaxy was obtained with the #1 0.9 m telescope of Kitt Peak National Observatory. This telescope is particularly suited to a study of Leo I because of its relatively large imaging field which is achieved without the use of a corrector, thus greatly reducing scattered light and ghost images from Regulus.

2. OBSERVATIONS

A field including the central part of Leo I was observed on the night of 1983 May 9 U.T., using CCD head No.6 attached to the f/7.5 Cassegrain focus of the #1 0.9 m telescope at Kitt Peak National Observatory (KPNO). The field was about 4.8' by 7.7', with a scale of 0.90 arcsec $pixel^{-1}$, and was centered 1.05' south, 1.29' west of the galaxy center. A 30 minute exposure was taken through each of B and V filters. The seeing for the exposures was 2.3 arcsec FWHM. The B exposure is shown in Figure 1.

Contamination by Regulus in the frames is minimal. There is a diffraction spike running across the centre of the field, rendering 2 or 3 rows (less than 1% of the frame) unuseable. The background appears to vary smoothly across the rest of the frame, presumably due to the aureole of Regulus. This, however, does not affect the determination of stellar brightnesses discussed in the next Chapter.

In practice, the CCD image as read out from the chip, contains a number of instrumental effects which should be removed before the proper reduction process can begin. This preprocessing was done for all data using software available at the telescope, following the standard procedure. First the zeropoint of the chip is set by subtracting the floating bias level (determined from overclocked pixels) for each frame. Next, a mean bias and a scaled dark frame are subtracted. A zero second exposure shows structure when it is read out. This is partly due to random readout noise (not repeatable), partly to certain electronic

Figure 1.

A 30 minute CCD exposure in B of Leo I. The size of the field is approximately 4.8' by 7.7'. North is to the right and east is up.

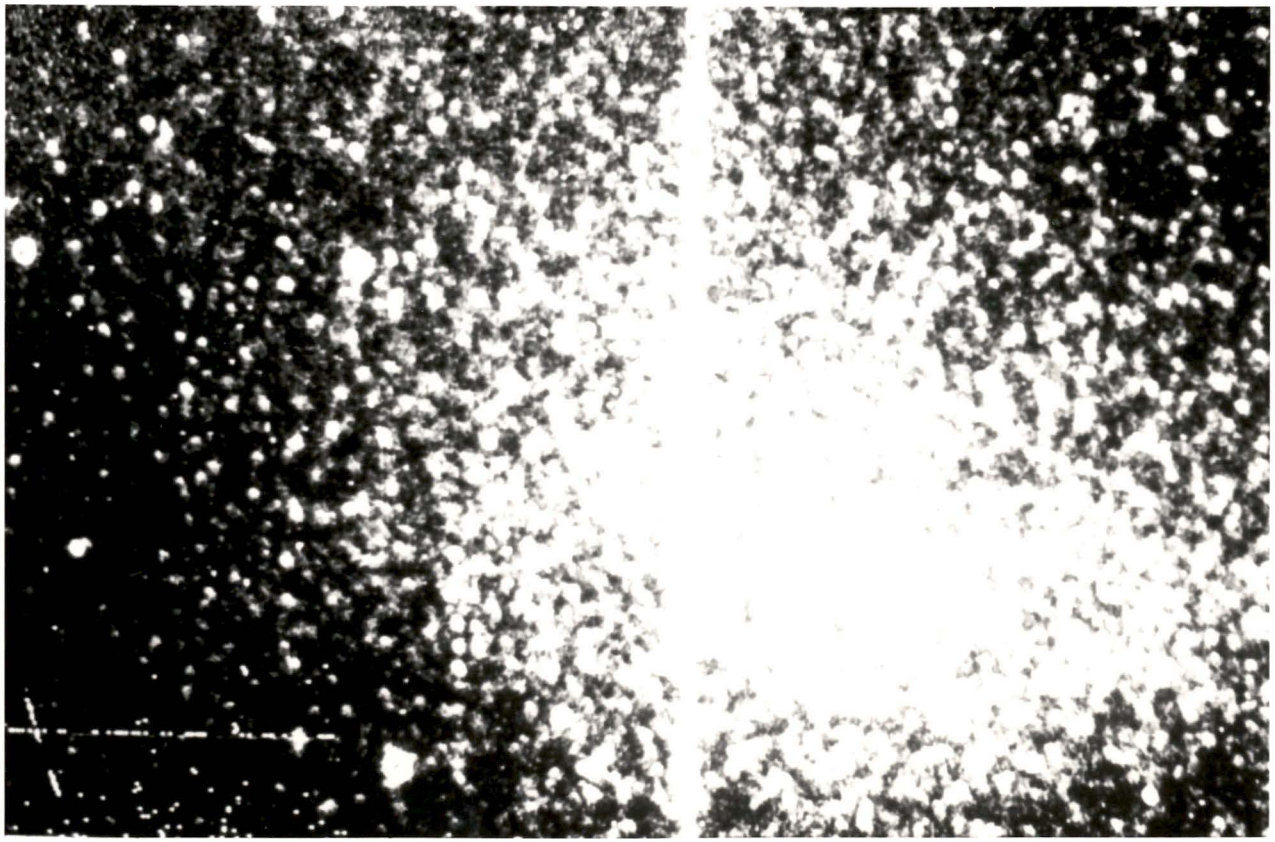

faults in reading out the chip. The electronic faults give rise to a bias that is constant for a particular chip. A mean is taken of several bias frames to minimize the effect of readout noise, and subtracted. Because of thermal diffusion, the wells will slowly accumulate electrons even without any incident light. This "dark" signal increases with time. It is measured by reading out the chip, leaving it unexposed for a known period of time and reading it out again. The frame obtained by this process is scaled to the exposure time of the data and subtracted.

Finally the observer must correct for pixel to pixel variations in sensitivity across the chip, i.e. flatten the field. The variations in sensitivity can arise from variations in pixel size or variations in the thickness of silicon above the pixel. Some exposures are taken of a uniformly lit surface, normally the inside of the telescope dome. Flat fields should be taken in each of the filters used for the observations, as the sensitivity may vary differently in different bandpasses. The data then divided by a normalised flat field in the same bandpass. Residual non-flatness of the dome flats is estimated to be ±1-2%, and does not affect the results that are discussed in the Chapters to follow.

3. ANALYSIS

Photometry

Crowding on the frames is moderate to severe (stellar surface density 0.01-0.1 arcsec^{-2}), requiring the use of a point spread function fitting program such as DAOPHOT (for a more complete description of the program see Appendix I). This program, developed by P. Stetson, simultaneously fits up to 60 stars with a predetermined point spread function, returning the least-squares coefficients and errors, along with shape and goodness of fit parameters for the stars that it has measured. These parameters allow a reasonably unbiased rejection scheme for poorly measured stars. The program also contains a fairly sophisticated star rejection scheme to eliminate spurious detections, such as cosmetic defects, cosmic rays and multiple hits on the same star.

Because of crowding problems, there was some difficulty finding relatively isolated stars from which to determine the point spread function (PSF) on each frame. Four or five stars were selected that appeared to be minimally crowded; these were among the brightest (unsaturated) stars in the field. From these, an initial guess at the PSF was made. This trial PSF was used to subtract contaminating stars, allowing the PSF to be improved. (The selected stars were contaminated by typically ~6 neighbours, all of which were significantly fainter than the PSF star.) This process was iterated until no improvement seemed to be achieved. (The final PSF appears to be excellent, as judged by the

residuals observed when all detected stars are subtracted from the frame.)

It is known that the PSF varied somewhat across the field of the KPNO #1 0.9m telescope at the time of the observations. When a mean PSF is used, as in the present work, this variation may lead to systematic errors in the stellar magnitudes. According to Stetson (1987), the effect introduces an error of $\sigma \simeq 0.03$ magnitudes in a typical worst case. From a comparison of aperture photometry and PSF-fitting photometry in one of the standard fields, it was possible to place an upper limit of $\sigma_{B-V} \leq 0.05$ magnitudes on the size of this effect in the Leo I frames. This value agrees with Stetson's, and is small compared to the errors in the photometry (see Table 2). In the discussion of the width of the giant branch (Chapter 5) therefore, this effect has not been considered.

A first pass through the star-finding routine located ~2200 stars in each frame. The brightnesses of these stars were measured approximately, and appropriately scaled PSF's were subtracted. The resulting picture was passed through the star-finding routine again to pick out faint stars that were previously concealed by brighter ones. This second pass increased the star lists to over 4000 stars. A third pass was attempted, but failed to increase the number of detections significantly.

The lists of 4000 stars were then subdivided into natural groups of no more than 60 stars each, and subsequently processed using the

NSTAR multiple profile fitting routine. A built-in star rejection scheme reduced the size of the lists to ~2200 stars in both the B and the V frames. The 1800 or so stars that were rejected were cases in which a star had been "found" twice, or objects that were too faint to be credible stars (i.e. random noise peaks). Although 1800 seems an excessively large number of spurious detections, it appears unavoidable when the degree of crowding varies this drastically across the frame. The DAOPHOT FIND threshold was set low enough to pick up real, faint stars in the uncrowded regions: this led to large numbers of spurious detections in more crowded regions.

The B and V frames were processed independently to avoid any colour bias. From the two lists of magnitudes that resulted (each containing ~2200 stars), 1326 matches were found by correlating objects in the V list with the closest object within 1 pixel in the B list. This was increased to 1601 matches by progressively allowing the critical separation to increase to 3 pixels, in an attempt to reach the horizontal branch. However, most of the "matches" at 1 to 3 pixels separation are spurious, increasing the scatter at the faint end of the diagram without clearly delineating the horizontal branch. The final list of stars therefore includes only those stars whose coordinates matched within 1.0 pixel. Although this matchup radius seems rather large, in fact it is only 40 percent of the FWHM. Furthermore, this list does not contain any stars with >1 candidate for matching within 1.0 pixel: five such stars were found, and were discarded.

Calibration

The instrumental magnitudes were transformed to the Johnson system using Landolt's (1973, 1983) equatorial standards, and the KPNO video camera standard field in M92 (Christian et al. 1985). Table 1 lists the observations of the standard fields. A total of 26 measurements was used, some stars being measured on more than one night. The data showed no night to night variation during the run (3 nights), so that standards observed on all 3 nights were used. The program field and the standard stars were observed at similar airmasses (1.19 to 1.27), so that differential extinction is relatively unimportant. The extinction coefficients were therefore taken from Bushouse (1985). The transformation equations derived from the standard star observations are:

$$V=v\ -0.015(\pm0.003)(B-V)\ -0.186(\pm0.041)(X-1)\ +24.61(\pm0.05)$$

$$B=b\ +0.201(\pm0.017)(B-V)\ -0.291(\pm0.048)(X-1)\ +24.97(\pm0.06)$$

where X denotes airmass. (The zeropoints are normalized to one second integration time and one airmass.) These values compare favourably with the work of Bushouse with the same detector. His values for the colour coefficients were -0.013 ± 0.004 in V and 0.187 ± 0.020 in B.

Completeness was tested by adding artificial stars at known magnitude and random (x,y) location, and repeating the entire measuring procedure. The point spread function of these artificial stars was identical to that empirically determined from the data. A total of 100

Table 1.

STANDARD FIELDS OBSERVED

Field	Number of Stars	Date (1983 UT)	Int. Time (sec)	Filter	Reference
SA 102	4	May 7	2	B	Landolt
			1	V	(1973, 1983)
SA 111	4	May 7	2	B	Landolt
			1	V	(1973, 1983)
SA 102	4	May 8	3	B	Landolt
			2	V	(1973, 1983)
VCAM M92	10	May 9	60	B	Christian et el.
			60	V	(1985)
VCAM M92	10	May 9	60	B	Christian et al.
			60	V	(1985)

stars were added at each of the magnitudes B=21, 22, 23 and 23.5, and V=20, 21, 22 and 23.

The accuracy with which DAOPHOT recovered artificial stars of known brightness also gives a much more realistic estimate of the errors of measurement than the formal error returned by the DAOPHOT NSTAR algorithm. For faint, crowded stars in particular, DAOPHOT considerably underestimates the error. Because of crowding problems, the number of stars recovered decreases from 90 percent at V=20 to 70 percent at V=22, and from 90 percent at B=21 to 35 percent at B=23. Below these magnitudes incompleteness increases steeply.

It was found, as expected, that both completeness and error are strongly dependent on position in the frames, since the degree of crowding varies substantially across the frame. To quantify this effect, the frames were divided into three zones of increasing stellar density, and the completeness and errors were reevaluated separately in each zone. Table 2 gives the completeness and r.m.s. error at each magnitude as a function of position in the frame. Note that although each zone is non-circular, it is roughly parametrized by the zonal radius given in Table 2.

The errors determined in this way are found to agree with those returned by the DAOPHOT NSTAR algorithm at brighter magnitudes ($\pm$0.07 mag at V=20). At fainter magnitudes the r.m.s. deviation from the known artificial star magnitudes rises above the formal DAOPHOT error. At V=22, it reaches 0.3, and continues to rise; no stars below this level were used in the final colour-magnitude diagram.

Table 2.

COMPLETENESS AND ERRORS

Filter	Mag	Severe Crowding*		Moderate Crowding†		Low Crowding‡	
		Completeness [percent]	Error [mag]	Completeness [percent]	Error [mag]	Completeness [percent]	Error [mag]
B	21	89 ± 7	0.14	94 ± 4	0.10	88 ± 5	0.08
	22	67 ±12	0.23	71 ± 8	0.27	85 ± 5	0.18
	23	14 ± 9	0.34	16 ± 6	0.34	46 ± 7	0.22
	23.5	<10	>0.5	15 ± 6	>0.5	16 ± 5	0.30
V	20	89 ± 7	0.11	97 ± 3	0.08	88 ± 5	0.07
	21	71 ±11	0.22	95 ± 3	0.23	79 ± 6	0.16
	22	50 ±12	0.43	67 ± 8	0.34	79 ± 6	0.30
	23	<10	>0.5	<10	>0.5	26 ± 6	0.32

* $0 \leq r ["] \leq 79$; $\langle n \rangle \sim 29$ stars arcmin^{-2} brighter than V=21.5

† $79 \leq r ["] \leq 167$; $\langle n \rangle \sim 18$ stars arcmin^{-2}

‡ $r ["] \geq 167$; $\langle n \rangle \sim 8$ stars arcmin^{-2}

4. THE COLOUR-MAGNITUDE DIAGRAM

Figure 2 shows the final colour-magnitude diagram (containing 575 stars; data for these stars are given in Appendix II), in which stars with low-quality measurements have been excised. A number of criteria was used to reject stars. First, stars that required ≥25 NSTAR iterations in both the B and V frames were considered not to have been measured accurately, and were eliminated. This criterion is a very conservative one, as DAOPHOT gives reasonably accurate magnitudes even after 25 iterations. All images with non-stellar shape were also removed from the list.

A further restriction was imposed based on the position in the field. As described in the previous Chapter, the field was (arbitrarily) divided into three regions of crowding. It was felt that those stars near the centre of the galaxy (i.e. those most severely crowded) were measured with significantly less accuracy than the stars in the outer two regions. All stars in the central, high stellar density area were therefore removed. (This covers only 14 percent of the total area of the frame.)

Finally, the formal error in the colour (B-V) (as returned by the DAOPHOT NSTAR algorithm) was used as a means of removing poorly measured stars. This error is an underestimate, as discussed above, and should not be confused with the true r.m.s. error quoted in Table 2. The final CMD has been plotted for the case in which the DAOPHOT uncertainty in (B-V) is less than 0.25. (From Table 2 the true r.m.s. error in (B-V)

Figure 2.

The best colour-magnitude diagram, containing 575 stars. The 7 carbon stars that appear in the diagram are marked with a different symbol. The formal uncertainty in (B-V) for all stars plotted is <0.25 magnitudes.

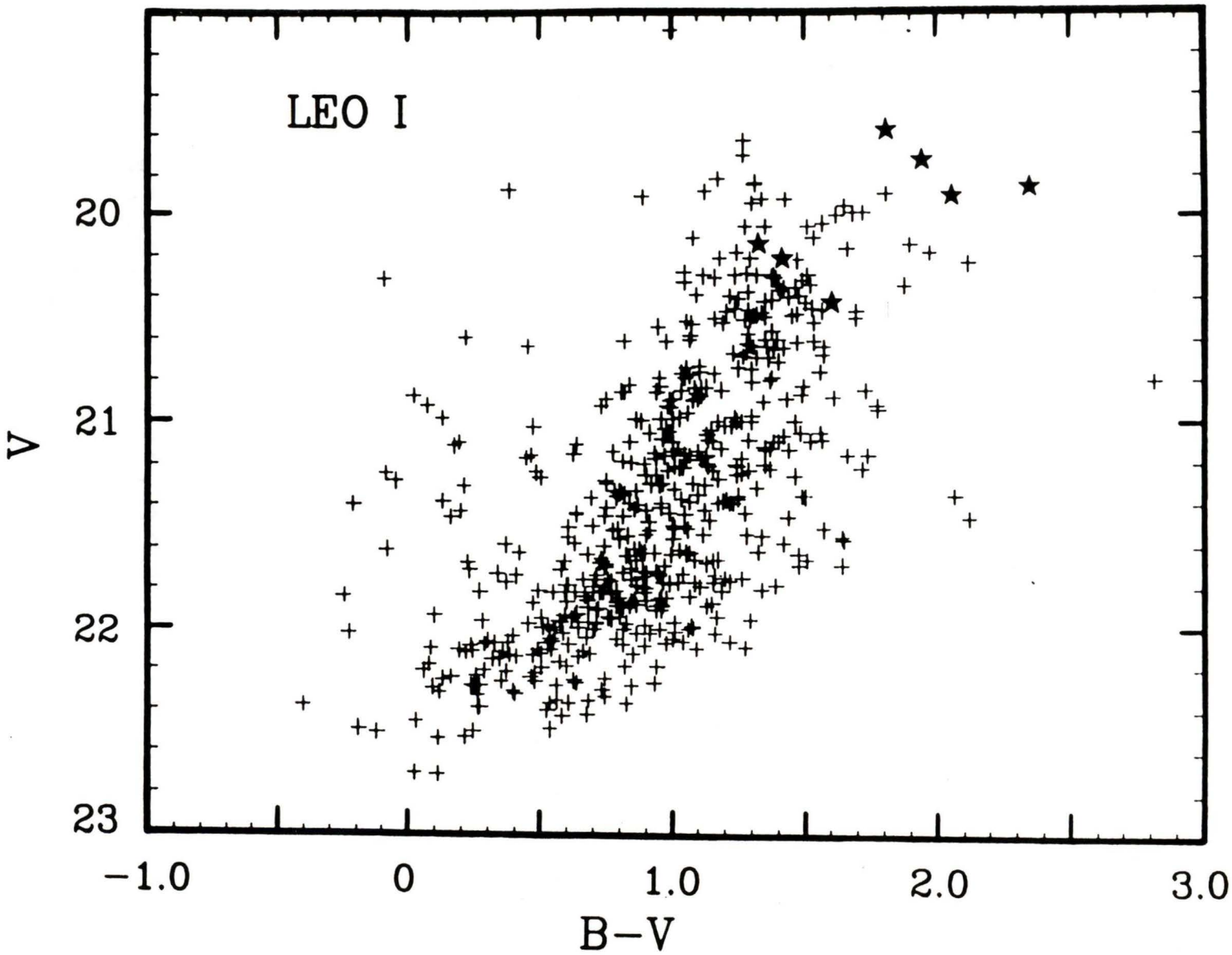
LEO I
20
21
22
23
V
−1.0
0
1.0
2.0
3.0
B−V

at the limit is estimated to be ~0.5 magnitudes.) The faintest stars in the diagram are well above the level below which completeness drops off catastrophically.

Interstellar reddening in the direction of Leo I is very low. Hodge and Wright (1978) do not correct for reddening; Zinn (1985) likewise quotes E(B-V) = 0.0. Webbink (1985) probably provides the most accurate determination, with a value E(B-V) = 0.02. In view of the accuracy of the photometry that is presented here, no correction for reddening has been made.

Contamination by field stars is expected to be minimal. From the star count models of Pritchet (1983), the total number of field stars in the field between magnitudes V=20 and V=22 is estimated to be ~15. Due to the selection procedures mentioned above, only ~7 of these will appear in the final diagram, out of a total of 575 stars.

5. DISCUSSION

Carbon Stars and the Age

Data for the 9 confirmed and 2 candidate carbon stars found by ALW which are in the field are presented in Table 3. ALW's star #1, a candidate carbon star, is found to be a double star, with a separation of 3.0 arcsec. Both components possess appropriate colours and magnitudes for carbon stars, so that at least one of the two is probably a carbon star. Of the resultant 12 confirmed or candidate carbon stars, 7 survived the selection procedures described in Chapter 4 (including both members of ALW #1), and these are plotted in Figure 2. The other 5, which were rejected by the selection procedures, nevertheless lie in the same area of the CMD.

Four of the seven candidate carbon stars appear to be the brightest stars (bolometrically) in the diagram, above the tip of the giant branch. The other three are just below the tip. The number of carbon stars, which are on the Asymptotic Giant Branch (AGB), at this magnitude level would seem to indicate a significant population of stars younger than typical globular cluster ages, although it is not possible to say which population is dominant. The height of these stars above the giant branch tip indicates an age of about 9 billion years (Iben and Renzini 1983), similar to the value found for the intermediate age population of most other dwarf spheroidal galaxies (e.g. Aaronson and Mould 1985, and references therein). For Leo I in particular, Aaronson and Mould (1985) find an age of around 9.5 billion years, based on

Table 3.

CARBON STAR DATA

ALW #*	V (mag)	error† (mag)	(B-V) (mag)	error† (mag)	Spectroscopically confirmed?	In Fig. 2?
1‡	20.42	0.04	1.61	0.08	no	yes
1‡	20.21	0.05	1.42	0.08	no	yes
2	19.72	0.02	1.95	0.06	yes	yes
5	19.97	0.04	1.27	0.07	yes	no
7	19.88	0.03	1.94	0.07	yes	no
8	19.86	0.03	1.05	0.06	yes	no
9	19.86	0.04	2.35	0.11	yes	yes
10	20.16	0.04	1.78	0.07	yes	no
11	20.14	0.23	1.33	0.25	yes	yes
12	20.46	0.04	2.07	0.15	no	no
14	19.58	0.03	1.81	0.05	yes	yes
15	19.90	0.03	2.05	0.06	yes	yes

* Identification number in Azzopardi, Lequeux and Westerlund (1985).

† Based on the formal errors returned by the DAOPHOT NSTAR routine.

‡ ALW star #1 is a double star; see text.

infrared observations of some of the carbon stars, which agrees very well with the present result (see also Suntzeff et al. 1986).

The Horizontal Branch

There is an apparent excess of faint blue ($V>22.0$, $(B-V)<0.6$) stars in the CMD. This is not due to incompleteness on the red side of the giant branch, as the cutoff is not determined by the limiting B magnitude, but rather by the error returned by DAOPHOT. Inspection of a CMD with all stars plotted also shows the excess. In this diagram, completeness is greater than 80% at this magnitude; the error is comparable on both the blue and red sides of the giant branch. Taken together, this evidence suggests that the feature is real. The obvious interpretation of this feature is that it is a horizontal branch, and indeed its magnitude level leads to a firm lower limit to the distance modulus of $(m-M)\geq 21.6$, if $M_V^{HB}=+0.6$ (e.g. Harris 1976, and references therein). This is in good agreement with other provisional determinations (see Chapter 1). Nevertheless, confirmation of this feature in the CMD of Leo I will require deeper CCD frames.

The Distance Modulus

There are two features in the CMD that allow a comparison with published mean ridge lines for galactic globular clusters (GC's), in order to estimate the distance to Leo I. First there is the tip of the

giant branch. All stars presumed to lie on the red giant branch (i.e. not the carbon stars) must be below the giant branch tip of the GC ridge lines. This gives an upper limit to the distance modulus. Secondly, the (absence of the) horizontal branch can be used. The position of the GC horizontal branch must be at or below the magnitude level of the group of stars identified above as evidence of a horizontal branch. This gives a lower limit to the distance modulus.

The best compromise found between these two indicators is shown in Figure 3. The ridge lines plotted are those for 47 Tuc (Hesser and Hartwick 1977) and for M13 (Sandage 1970), which bracket the data. The distance modulus of 47 Tuc is taken to be (m-M)=13.14 (Lee 1977, with M_V^{HB}=+0.8) and that of M13 is (m-M)=14.33 (Harris and Racine 1979). This gives an estimate of the distance to Leo I, which is found to be 21.8 ± 0.2. This is in good agreement with the traditional estimate of 21.7, obtained by Hodge (1966) from the magnitude of the brightest member stars.

The Metallicity

Near the bright end of the giant branch, the errors in colour are small ($\sigma_{B-V} \leq 0.1$ magnitudes). The observed scatter of the data about the ridge line, however, shows a σ_{B-V} of ~0.25 magnitudes. This clearly demonstrates the anomalous width of the giant branch compared to that of globular clusters ($\sigma_{B-V} \leq 0.05$ magnitudes). The width must be primarily due to a spread in composition, as age and other parameters do not affect the morphology of the tracks significantly at this location in

Figure 3.

As in Figure 2, with the sequences for 47 Tuc (lower) and M13 (upper) superimposed. The globular cluster CMD's include both giant branch and asymptotic giant branch, and the horizontal branch.

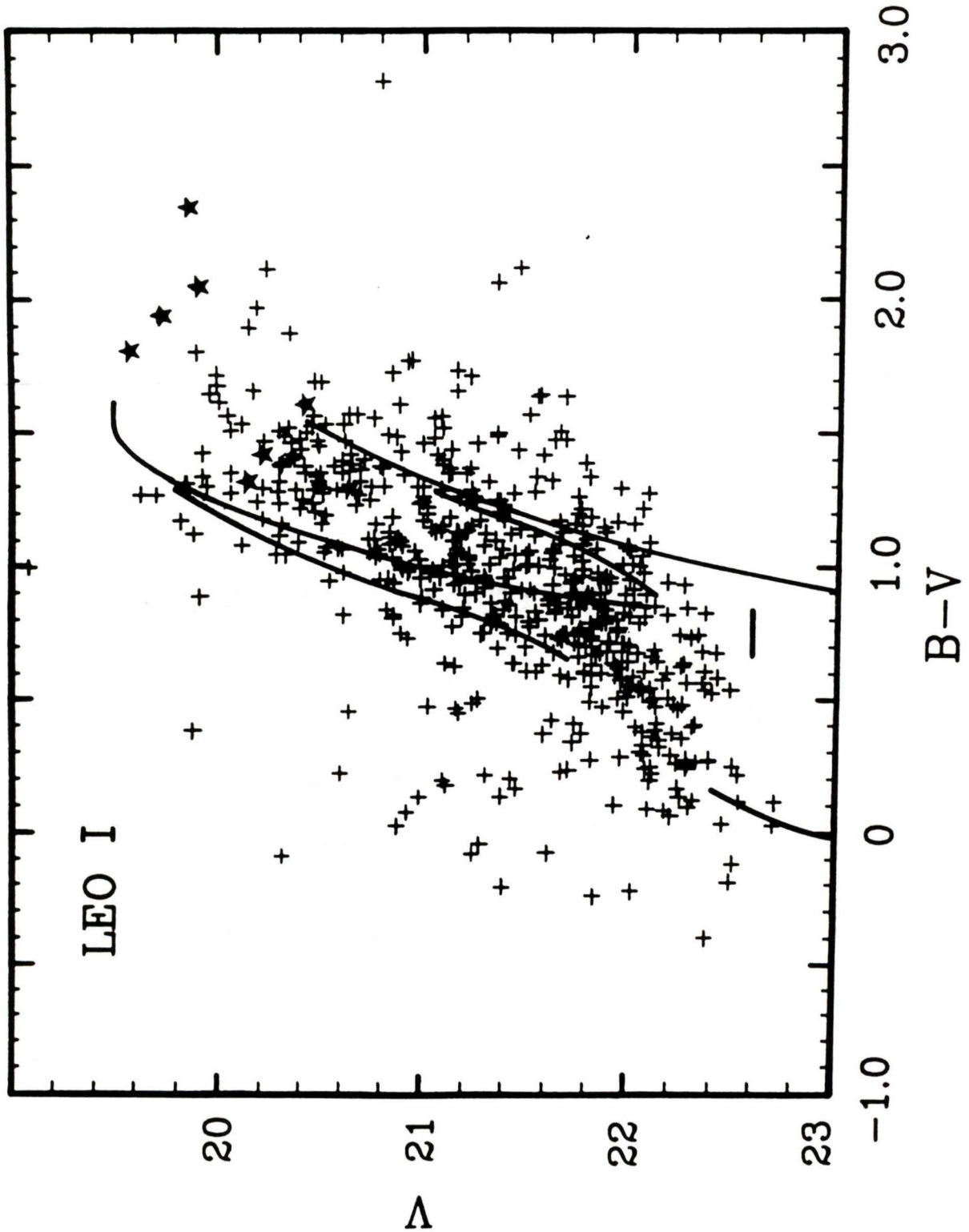
LEO I
V
B−V
20
21
22
23
−1.0
0
1.0
2.0
3.0

the CMD. Figure 3 then shows the metallicity of Leo I to vary between the metallicities of the two globular clusters plotted. The distribution of stars near the 47 Tuc ridge line indicates that the upper limit to the metallicity is not well defined. There appear to be small numbers of stars with quite high metallicities, but the total number with metallicity higher than that of 47 Tuc would seem to be very small indeed.

Comparison of the diagram with the theoretical red giant branches of VandenBerg (1984) is presented in Figure 4. The tracks have been shifted in V by (m-M)=21.8. The VandenBerg (1984) calculations show agreement with the current data if the spread in metallicity in the galaxy is from approximately [Fe/H]=-1.8 to [Fe/H]=-0.8. Although subject to the vagaries of the uncertain zero-point of the globular cluster abundance scale, this result is in reasonable accord with abundances for the two globular cluster sequences plotted in Fig. 3 (cf. [Fe/H]=-0.71 for 47 Tuc versus [Fe/H]=-1.65 for M13, Zinn and West 1984). The mean metallicity, weighted by the number of stars at each value, appears to be near [Fe/H]=-1.4. Suntzeff et al. (1986) obtained a value of [Fe/H]=-1.5 ± 0.25 from spectroscopy of 2 giants. In spite of the very small sample of objects observed, their result is consistent with that found above; nevertheless, spectroscopic determinations of the metal abundance of many more Leo I giants would be very useful to verify the abundance spread observed here.

The CMD's obtained by Demers and Harris (1983) for Leo II and by Demers et al. (1979) for Fornax both are morphologically very similar to

Figure 4.

As in Figure 2, with the VandenBerg (1984) theoretical red giant branches superimposed. The giant branches have been truncated at (B-V)=1.7 due to uncertainties in the bolometric corrections beyond this point. Metallicities for the plotted tracks are (from bottom to top): -0.49, -0.79, -1.27, -1.77, and -2.27

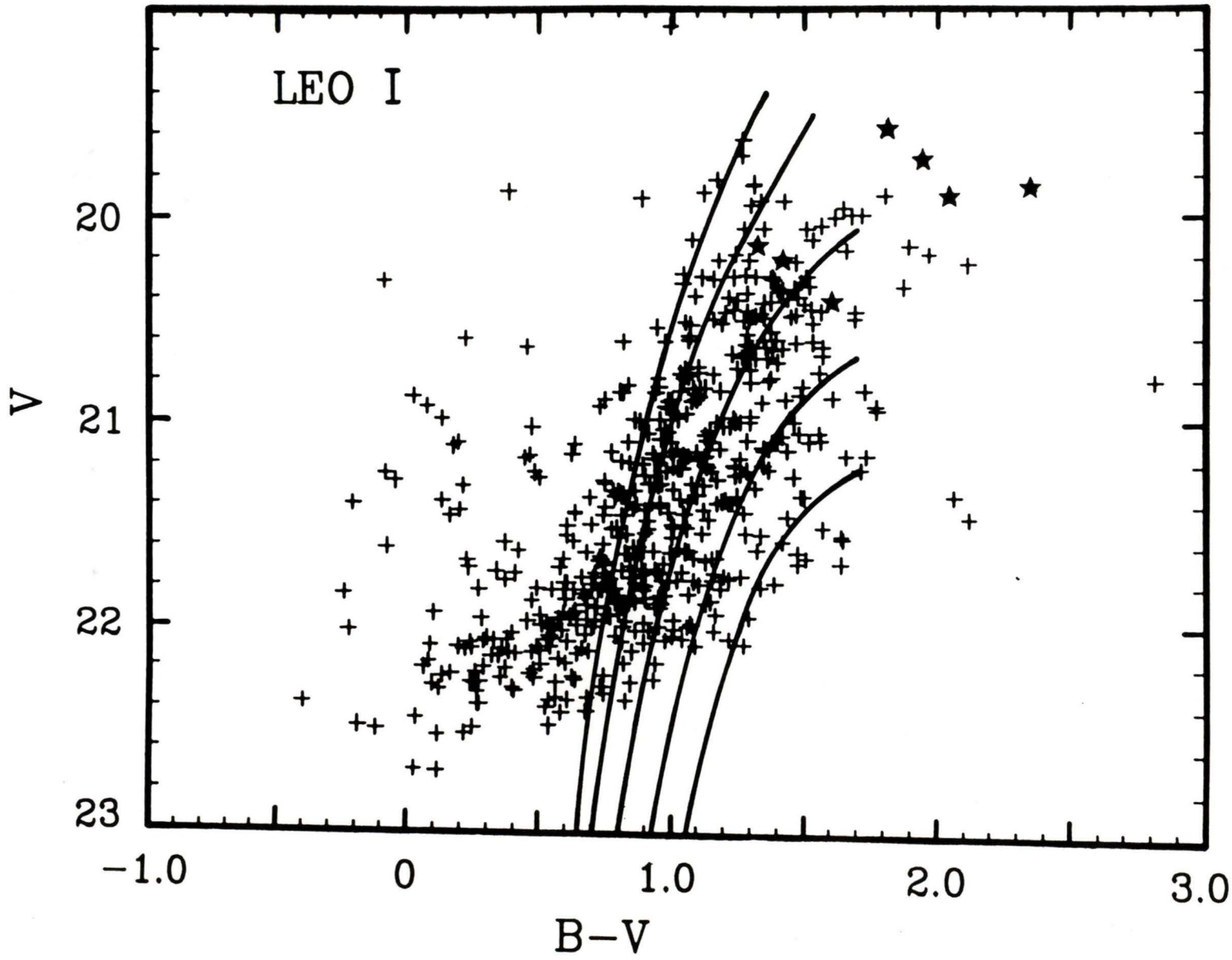
LEO I
V
20
21
22
23
−1.0
0
1.0
2.0
3.0
B−V

the CMD for Leo I. All three exhibit a red giant branch of similar width, red extent, and slope. The slope seems to be the most discrepant of the three parameters, in the sense that Fornax has a slightly shallower giant branch. This indicates a slight variation in metallicity amongst these three dwarf spheroidals, with Fornax being more metal rich. It is interesting to note that the upper giant branches of Ursa Minor and Draco, the two most metal poor members of the dwarf spheroidal family, have quite a different appearance. Not only are they considerably steeper, but the width is significantly reduced. As the Leo dwarfs and Fornax are the most luminous and the most massive dwarf spheroidals, it would be useful to extend the comparison to fainter magnitudes. If fainter features in the CMD are also similar, it could provide us with clues to the origin of these peculiar galaxies.

6. CONCLUSION

A CMD is presented for the dwarf spheroidal galaxy Leo I, reasonably complete down to V=22. A prominent giant branch is visible, and the existence is confirmed of a significant population of AGB stars above the giant branch. From a comparison of the results with (i) the ridge lines for various globular clusters, and (ii) theoretical red giant branches, the traditional distance modulus of $(m-M)=21.8 \pm 0.2$ is confirmed. The mean metallicity of the system is estimated to be [Fe/H] = -1.4, in reasonable agreement with previous determinations. However, the width and shape of the giant branch provides clear evidence for a very large spread (± 0.5 dex) in the metallicity.

Further work is obviously required to extend the CMD of Leo I to fainter magnitudes, since a comparison of the CMD's of the Leo dwarfs with that of Fornax may provide us with clues to the origin of these systems. First of all, the type of horizontal branch is unknown for Leo I. At present only the Ursa Minor dwarf is known to possess a blue horizontal branch. Since $V_{HB} \leq 22.5$, this observation should now be quite straightforward with reasonably short integration times. In addition, observations of the main sequence turnoff are of great importance, since such observations could in principle determine the star formation history of Leo I. Finally, spectroscopic observations of Leo I giants might provide interesting clues to the chemical evolution of this dwarf galaxy, and, by inference, of dwarf galaxies in general.

BIBLIOGRAPHY

Aaronson, M. and Mould, J.R. (1985). Astrophys. J. 290, 191.

Aaronson, M., Olszewski, E.W. and Hodge, P.W. (1983). Astrophys. J. 267, 271.

Azzopardi, M., Lequeux, J. and Westerlund, B.E. (1985). Astron. Astrophys. 144, 388 (ALW).

Bushouse, H. (1985). N.O.A.O. Newsletters No. 4, p.14.

Christian, C.A., Adams, M., Barnes, J.V., Butcher, H., Hayes, D.S., Mould, J.R. and Siegel, M. (1985). Publ. Astron. Soc. Pac. 97, 363.

Demers, S. and Harris, W.E. (1983). Astron. J. 88, 329.

Demers, S., Kunkel, W.E. and Hardy, E. (1979). Astrophys. J. 232, 84.

Harrington, R.G. and Wilson, A.G. (1950). Publ. Astron. Soc. Pac. 62, 118.

Harris, W.E. (1976). Astron. J. 81, 1095.

Harris, W.E. and Racine, R. (1979). Annu. Rev. Astron. Astrophys. 17, 241.

Hesser, J.E. and Hartwick, F.D.A. (1977). Astrophys. J. Suppl. 33, 361.

Hodge, P.W. (1966). Astrophys. J. 174, 557.

Hodge, P.W. (1986). Galaxies (Harvard University Press, Cambridge, Massachusetts).

Hodge, P.W. and Wright, F.W. (1978). Astron. J. 83, 228.

Iben, I. Jr. and Renzini, A. (1983). Annu. Rev. Astron. Astrophys. 21, 271.

Knapp, G.R., Kerr, F.J. and Bowers, P.F. (1978). Astron. J. 83, 360.

Landolt, A.U. (1973). Astron. J. 78, 959.

Landolt, A.U. (1983). Astron. J. 88, 439.

Lee, S.W. (1977). Astron. Astrophys. Suppl. 27, 381.

Pritchet, C.J. (1983). Astron. J. 88, 1476.

Sandage, A. (1970). Astrophys. J. 162, 841.

Stetson, P.B. (1987). Private communication.

Suntzeff, N.B., Aaronson, M., Olszewski, E.W. and Cook, K.H. (1986). Astron. J. 91, 1091.

VandenBerg, D.A. (1984). In Observational Tests of the Stellar Evolution Theory, IAU Symposium No. 105, edited by A.Maeder and A.Renzini (Reidel, Dordrecht), p. 143.

Webbink, R.F. (1985). In Dynamics of Star Clusters, IAU Symposium No. 113, edited by J.Goodman and P.Hut (Reidel, Dordrecht), p. 541.

Zinn, R. (1985). Mem. Soc. Astron. Ital. 56, 223.

Zinn, R. and West, M.J. (1984). Astrophys. J. Suppl. 55, 5.

APPENDIX I DAOPHOT

The computer program called DAOPHOT was employed to measure the magnitudes of stars in the field. It was written by P.B. Stetson of the Dominion Astrophysical Observatory (DAO), and is generally considered to be one of the best of its kind. The strength of the program lies in its ability to deal with blended images. It can accurately recover stellar magnitudes even when several images are closely blended. Thus fields previously considered to be hopelessly crowded, fields where conventional aperture photometry is quite impossible are now open to investigation.

The structure is that of a command language: on running the program, the user enters an environment where DAOPHOT commands can be entered. Each command performs one step of the reduction procedure. The results of each step can be examined before proceeding to the next. If necessary a step, or a group of steps, can be repeated until satisfactory results are achieved. On the following pages a short description will be given of the most important commands. Not all of the commands are listed, however. The intention is to provide an understanding of the algorithms rather than a complete user manual.

The input required by DAOPHOT is a CCD frame in the Shortridge/Mould (Caltech) data-structure file format. The response of the CCD is assumed to be linear. Subtraction of the bias level and flatfielding should be done before entering the DAOPHOT environment. Immediately after running the program, some parameters need to be

initialized, e.g. the photon to Digital Unit conversion factor during operation of the CCD, the readout noise per pixel of the chip and the size of the seeing disk in pixels. Then the reduction process proper can begin.

FIND The command FIND first convolves the frame with a gaussian whose FWHM is specified in the initial set up parameters. Effectively this reduces the size of the random noise peaks, making it easier to pick out the real stars. It then searches through the frame for significant peaks; the limit of significance is supplied by the user. Note that the procedure is most efficient for stars whose FWHM is close to that of the gaussian used in the convolution. The output is a list of rough star positions.

PHOT Having found stars with the FIND routine, one then proceeds to estimate the brightness of each. The command PHOT will perform aperture photometry on each of the stars. Of course, in a crowded field this photometry will be very crude indeed, but an initial guess is required to speed up the profile fitting routines later. For this purpose, aperture photometry is adequate. The output from PHOT is a list of (improved) coordinates and crude magnitudes.

PSF A crucial part of the reduction with DAOPHOT is defining the Point Spread Function (PSF). The PSF describes the way the atmosphere spreads out the light from a point source (e.g. a star). It is

defined as the shape of an image of a point source. In an uncrowded field it is therefore the shape of any of the stars. In a crowded field however, it is the shape of a single star. It is necessary to have bright, isolated stars to determine the PSF properly. Depending on the degree of crowding, it may be difficult to find suitable stars. The best candidates available (about 6 are required for an accurate PSF) should be located by visual inspection of the frame. These stars should then be input to the PSF command. An average profile is determined from the selected stars, which serves as a first approximation of the PSF. Faint stars contaminating the selected stars may be subtracted out, and the process iterated to improve the PSF. When the user is satisfied with the PSF found, a file is created containing the empirically determined profile. This file is required as input to all of the profile fitting routines to follow.

PEAK The command PEAK is a routine for doing photometry using single profile fits. It requires as input a list of coordinates with rough magnitudes (e.g. output from PHOT) and a PSF. The routine performs a least-squares fit of the PSF to each of the stars in the list individually. As such, it is more accurate than the PHOT command and even works very well in uncrowded fields. In crowded fields however, the magnitudes are not recovered accurately enough due to contamination from neighbouring stars. The output is a list of improved coordinates and magnitudes.

Following the command PEAK it is usually a good idea to subtract out all of the stars found thus far. This enables faint stars, previously concealed by brighter ones to be found with the FIND routine. A rough estimate of the magnitudes of the new stars is found using PHOT, and this data is added to the file containing the previous photometry. The subtraction and finding may be iterated as necessary, although two passes through FIND is normally sufficient to detect all stars for which useful information can possibly be recovered. With a file containing crude magnitudes for all of the stars found on the frame, the user can prepare to do the multiple profile fits.

GROUP Before actually doing the multiple fit, the stars in the data file need to be sorted into natural groups. The multiple profile fitting routine solves a group of stars simultaneously. Therefore any two stars that are within a critical radius of each other need to be in the same group. The command GROUP performs this task, reorganizing the entries in a photometry file. All information is preserved, i.e. positions and magnitudes. The critical separation is supplied by the user; it should be large enough so that two stars separated by the critical separation no longer contribute a significant amount of light to each other. On the other hand it should be as small as possible to give smaller groups, which are reduced faster by the multiple profile fitting routine. In any case, the maximum number of stars allowed in a single group for the multiple fit is 60. Any groups larger than this need to be broken down further.

NSTAR The routine that performs the multiple fits is called NSTAR. It is the part of the reduction procedure where the actual measuring is done. As input, it requires a file containing stellar groups, e.g. output from GROUP, and a file containing the empirical PSF. Each star should have coordinates and a rough magnitude. One group at a time, NSTAR performs a simultaneous least squares fit of the PSF to each of the stars in the group. Both the coordinates and the magnitudes are improved iteratively until all of the stars in a group meet very strict convergence criteria. Stars may be deleted (automatically) from the group if they fade out of existence during the iterative procedure, or if they merge with a brighter star in the group. The criteria used to delete stars are such that spurious detections and multiple hits on the same star are eliminated from the final star list. The output is a list of stars with accurate coordinates, instrumental magnitudes and some parameters with information on the goodness of fit. These parameters may be used to weed out poor measurements, e.g. objects with non-stellar shape (galaxies), saturated stars etc.

Because NSTAR rejects some of the detections, it may be desirable to re-GROUP the stars with a larger critical separation and repeat the NSTAR command. If the signal to noise ratio is low, this procedure could improve the accuracy of the final photometry. In any case, when the user is satisfied that the program has extracted the maximum amount of information from the frame, there are some tests that can be done to check the quality of the photometry. Some of the goodness of fit

parameters behave in a predictable way if the procedure was executed correctly. These may be used as a check. The stars may also be subtracted from the frame, according to the PSF and the magnitudes returned by NSTAR. If the measurements are accurate, the residual field should be completely flat. Any deviation from flatness immediately indicates a problem. For individual stars, this is acceptable, but if all of the stars show non-flat residuals, the PSF was not determined properly. In this case the entire procedure should be repeated.

APPENDIX II THE DATA

ID	X	Y	V (mag)	B-V (mag)	σ_V (mag)	σ_{B-V} (mag)
1	201.59	5.19	21.442	0.637	0.108	0.153
2	172.97	6.36	21.663	0.591	0.091	0.143
3	164.56	6.17	21.620	0.893	0.170	0.245
4	102.71	6.37	20.600	1.350	0.040	0.075
5	300.73	6.46	21.856	0.900	0.138	0.239
6	15.69	7.15	20.623	1.281	0.045	0.071
7	132.91	7.67	21.240	0.486	0.065	0.104
8	228.64	8.50	20.690	1.321	0.090	0.117
9	122.00	9.25	20.996	1.463	0.046	0.112
10	247.30	9.82	21.159	0.970	0.093	0.143
11	270.13	9.62	21.348	1.101	0.072	0.153
12	262.78	10.83	21.724	1.042	0.101	0.210
13	253.12	10.58	21.974	0.897	0.116	0.225
14	144.35	13.16	22.177	0.942	0.137	0.217
15	128.97	13.11	21.755	0.755	0.088	0.136
16	309.62	13.48	21.745	1.265	0.089	0.228
17	151.41	14.23	19.983	1.719	0.031	0.070
18	283.57	14.67	21.639	0.836	0.116	0.171

APPENDIX II (cont.)

ID	X	Y	V (mag)	B-V (mag)	σ_V (mag)	σ_{B-V} (mag)
19	238.00	16.74	21.709	0.888	0.108	0.164
20	263.50	16.83	21.830	0.671	0.153	0.198
21	42.58	17.04	21.628	1.476	0.096	0.194
22	258.20	18.10	22.029	0.394	0.149	0.234
23	157.83	19.41	21.558	0.801	0.088	0.162
24	132.34	19.60	21.155	1.738	0.097	0.204
25	96.20	21.10	21.057	1.131	0.063	0.107
26	111.55	20.97	21.045	0.915	0.089	0.131
27	143.10	21.43	20.519	1.534	0.062	0.113
28	28.01	21.99	20.969	1.303	0.061	0.124
29	307.44	22.39	19.953	1.651	0.027	0.059
30	37.99	23.20	21.702	0.577	0.112	0.136
31	141.88	24.12	20.384	1.091	0.067	0.095
32	50.75	24.44	20.209	1.181	0.053	0.082
33	236.24	25.52	19.903	2.050	0.031	0.060
34	255.29	25.78	20.887	1.430	0.068	0.157
35	275.18	26.25	20.832	1.085	0.057	0.092
36	48.02	26.36	20.035	1.565	0.050	0.084
37	257.75	27.01	20.616	1.470	0.075	0.150
38	80.13	28.80	21.414	0.857	0.059	0.098

APPENDIX II (cont.)

ID	X	Y	V (mag)	B-V (mag)	σ_V (mag)	σ_{B-V} (mag)
39	88.07	28.82	21.043	0.991	0.066	0.095
40	95.63	29.27	20.739	1.249	0.045	0.074
41	248.56	29.17	20.448	1.525	0.035	0.079
42	257.82	30.12	20.463	1.695	0.085	0.145
43	66.40	31.07	20.691	1.364	0.050	0.090
44	283.44	32.43	21.547	1.642	0.095	0.216
45	113.93	32.65	21.654	1.173	0.094	0.176
46	265.81	33.74	20.601	1.067	0.045	0.080
47	65.65	34.12	21.207	1.139	0.081	0.122
48	10.03	34.49	20.634	1.360	0.065	0.110
49	22.19	34.42	21.739	0.888	0.117	0.194
50	53.16	34.33	21.650	0.731	0.081	0.133
51	246.44	34.80	21.712	0.938	0.141	0.191
52	147.83	35.45	20.862	1.488	0.053	0.113
53	236.39	35.45	20.289	1.383	0.048	0.105
54	261.80	36.68	21.047	1.486	0.089	0.146
55	82.11	36.65	21.388	1.231	0.066	0.134
56	288.01	38.47	20.936	1.776	0.067	0.173
57	109.77	38.96	20.595	0.220	0.032	0.047
58	135.35	39.93	21.435	1.278	0.090	0.194

APPENDIX II (cont.)

ID	X	Y	V (mag)	B-V (mag)	σ_V (mag)	σ_{B-V} (mag)
59	22.19	39.82	20.161	1.658	0.041	0.072
60	30.66	40.26	19.995	1.619	0.045	0.067
61	141.49	40.87	21.574	1.421	0.077	0.223
62	85.86	41.34	21.664	0.738	0.131	0.164
63	176.34	41.57	21.496	0.698	0.089	0.128
64	90.85	42.69	21.815	0.633	0.090	0.145
65	169.66	43.60	21.225	1.716	0.084	0.176
66	230.44	43.25	21.428	0.200	0.095	0.112
67	147.94	44.02	20.799	1.370	0.062	0.105
68	110.34	44.68	20.804	1.303	0.053	0.093
69	274.48	45.50	21.079	1.563	0.075	0.132
70	113.39	45.67	20.822	0.954	0.044	0.079
71	7.80	47.09	20.781	1.379	0.049	0.092
72	296.15	49.64	19.080	0.996	0.029	0.036
73	143.97	49.89	20.454	1.235	0.051	0.077
74	304.19	50.12	21.997	0.705	0.166	0.218
75	162.12	50.22	21.393	-0.208	0.103	0.116
76	85.82	50.76	21.832	1.064	0.107	0.176
77	191.57	51.89	21.949	1.294	0.129	0.226
78	39.66	51.14	21.769	0.989	0.137	0.244

APPENDIX II (cont.)

ID	X	Y	V (mag)	B-V (mag)	σ_V (mag)	σ_{B-V} (mag)
79	164.94	52.31	21.546	0.606	0.113	0.160
80	43.73	52.03	20.648	1.382	0.061	0.099
81	274.85	53.15	21.089	1.522	0.074	0.119
82	310.07	53.40	21.202	1.134	0.079	0.186
83	237.48	54.79	21.784	1.107	0.097	0.164
84	119.02	54.48	21.355	1.500	0.090	0.186
85	241.28	55.15	20.848	0.943	0.107	0.128
86	27.26	55.27	20.888	0.751	0.056	0.090
87	163.22	55.52	20.680	1.267	0.048	0.091
88	142.87	56.51	21.293	0.965	0.080	0.130
89	282.19	57.37	21.328	0.802	0.173	0.228
90	176.40	60.15	21.624	1.069	0.103	0.158
91	14.54	60.57	21.724	0.948	0.099	0.149
92	116.54	60.84	21.176	1.109	0.061	0.104
93	192.69	61.26	19.936	1.301	0.028	0.056
94	49.86	62.58	22.701	0.024	0.150	0.202
95	179.07	62.47	20.852	0.820	0.059	0.093
96	307.99	63.24	20.760	1.034	0.057	0.098
97	220.05	63.98	21.370	1.205	0.076	0.174
98	315.34	64.01	21.034	1.147	0.059	0.118

APPENDIX II (cont.)

ID	X	Y	V (mag)	B-V (mag)	σ_V (mag)	σ_{B-V} (mag)
99	280.08	65.32	20.819	0.836	0.060	0.086
100	136.60	66.74	21.897	0.721	0.175	0.222
101	185.77	67.08	21.719	0.902	0.123	0.204
102	84.46	68.44	21.228	0.984	0.083	0.117
103	219.23	68.14	21.310	1.319	0.085	0.172
104	99.55	71.03	21.612	1.029	0.132	0.184
105	90.10	71.50	20.510	1.054	0.040	0.083
106	72.87	73.98	22.313	0.405	0.164	0.213
107	31.89	75.10	20.990	1.245	0.039	0.111
108	268.75	75.27	20.308	-0.090	0.042	0.052
109	113.13	75.82	20.728	1.105	0.051	0.076
110	197.29	76.58	21.249	0.900	0.054	0.122
111	40.26	77.10	21.634	0.825	0.088	0.192
112	67.86	77.26	22.284	0.093	0.143	0.176
113	47.24	79.21	20.610	1.533	0.054	0.088
114	268.44	80.14	20.460	1.290	0.097	0.159
115	115.79	80.35	20.978	0.131	0.086	0.109
116	105.19	81.60	21.994	0.950	0.145	0.245
117	66.80	82.90	20.414	1.349	0.039	0.067
118	39.62	83.40	20.983	0.956	0.072	0.101

APPENDIX II (cont.)

ID	X	Y	V (mag)	B-V (mag)	σ_V (mag)	σ_{B-V} (mag)
119	43.49	83.92	20.828	1.129	0.055	0.095
120	81.58	83.93	21.961	1.007	0.135	0.234
121	23.24	84.28	22.262	0.635	0.157	0.224
122	130.85	86.54	19.576	1.813	0.026	0.049
123	53.59	88.18	21.938	0.757	0.129	0.181
124	48.97	89.81	21.131	1.350	0.059	0.120
125	118.98	91.16	22.306	0.118	0.210	0.245
126	146.36	90.75	17.832	0.975	0.035	0.044
127	156.57	91.28	20.337	1.520	0.046	0.105
128	102.49	91.72	21.839	0.979	0.111	0.179
129	134.02	92.68	22.058	1.216	0.159	0.240
130	124.81	92.66	22.488	-0.190	0.152	0.179
131	84.07	93.92	20.468	1.205	0.046	0.075
132	90.03	95.70	22.202	0.060	0.131	0.197
133	310.59	97.92	20.879	1.607	0.057	0.170
134	92.85	99.06	21.972	0.455	0.109	0.158
135	137.11	99.08	21.357	0.693	0.086	0.119
136	78.08	102.35	22.258	0.931	0.154	0.232
137	122.91	102.51	21.138	0.775	0.104	0.136
138	56.80	102.58	20.368	1.285	0.046	0.118

APPENDIX II (cont.)

ID	X	Y	V (mag)	B-V (mag)	σ_V (mag)	σ_{B-V} (mag)
139	67.50	102.61	20.635	0.453	0.044	0.054
140	126.13	102.84	22.120	0.504	0.181	0.237
141	40.49	103.28	22.709	0.109	0.196	0.249
142	93.37	103.38	20.976	1.031	0.050	0.089
143	126.65	106.59	22.061	0.378	0.156	0.187
144	77.16	107.32	21.111	0.176	0.052	0.127
145	47.32	110.75	22.204	0.372	0.123	0.175
146	16.26	112.54	21.156	1.011	0.063	0.122
147	310.03	113.39	20.498	1.692	0.041	0.118
148	67.28	113.16	21.380	0.134	0.087	0.113
149	79.74	116.97	20.954	1.059	0.066	0.102
150	66.14	116.80	20.507	1.272	0.046	0.079
151	124.16	117.40	22.323	0.264	0.155	0.209
152	17.16	120.22	21.980	1.074	0.171	0.240
153	81.45	125.05	19.987	1.680	0.034	0.064
154	307.94	126.32	21.165	1.128	0.089	0.152
155	75.45	127.85	20.919	0.982	0.045	0.084
156	24.33	128.15	20.292	1.120	0.041	0.061
157	105.91	127.93	21.270	1.176	0.086	0.147
158	33.50	129.26	21.746	1.196	0.095	0.210

APPENDIX II (cont.)

ID	X	Y	V (mag)	B-V (mag)	σ_V (mag)	σ_{B-V} (mag)
159	92.50	129.58	21.929	0.591	0.147	0.200
160	89.03	129.75	21.959	0.711	0.122	0.185
161	44.79	129.80	20.289	1.321	0.053	0.079
162	160.22	131.12	21.511	0.792	0.091	0.141
163	56.85	130.96	21.087	1.380	0.060	0.121
164	103.16	130.98	20.051	1.348	0.032	0.063
165	149.47	132.27	20.340	1.876	0.073	0.161
166	317.44	132.04	20.140	1.327	0.229	0.245
167	37.50	132.29	21.998	0.815	0.152	0.229
168	29.99	135.12	21.945	0.619	0.123	0.181
169	110.34	136.25	20.487	1.452	0.044	0.088
170	90.87	136.18	22.242	0.745	0.153	0.229
171	146.01	137.96	19.623	1.271	0.027	0.040
172	114.28	138.46	22.125	0.382	0.147	0.222
173	75.26	139.68	21.815	0.701	0.096	0.146
174	36.21	140.12	21.047	1.557	0.052	0.114
175	94.95	140.23	20.413	1.378	0.044	0.081
176	32.72	141.39	22.017	0.865	0.121	0.208
177	123.19	141.80	21.561	1.645	0.109	0.224
178	98.31	142.75	20.890	1.082	0.068	0.100

APPENDIX II (cont.)

ID	X	Y	V (mag)	B-V (mag)	σ_V (mag)	σ_{B-V} (mag)
179	129.36	144.84	21.860	0.601	0.088	0.127
180	315.91	144.55	21.815	0.724	0.160	0.229
181	133.27	145.11	21.324	0.862	0.075	0.105
182	105.61	145.25	20.291	1.238	0.050	0.077
183	10.01	145.27	21.792	0.900	0.089	0.201
184	114.25	146.22	19.855	2.350	0.044	0.114
185	14.37	147.94	20.350	1.423	0.052	0.086
186	71.84	148.16	20.470	1.338	0.039	0.078
187	152.37	149.12	20.841	1.188	0.045	0.096
188	64.63	150.57	21.455	1.438	0.106	0.204
189	67.40	152.43	22.143	0.319	0.161	0.218
190	45.88	153.88	21.778	1.390	0.077	0.155
191	120.71	154.09	21.191	0.844	0.065	0.098
192	9.96	155.90	22.177	0.599	0.138	0.215
193	25.69	157.04	21.658	1.508	0.100	0.250
194	155.01	156.61	22.099	0.542	0.147	0.184
195	33.86	161.60	21.966	0.825	0.157	0.204
196	73.93	162.70	20.104	1.532	0.023	0.148
197	79.52	162.98	21.939	0.503	0.119	0.149
198	306.83	163.33	19.914	1.336	0.039	0.064

APPENDIX II (cont.)

ID	X	Y	V (mag)	B-V (mag)	σ_V (mag)	σ_{B-V} (mag)
199	83.45	165.98	21.175	1.056	0.073	0.121
200	46.62	166.65	21.734	1.161	0.119	0.185
201	137.76	168.15	19.816	1.171	0.026	0.043
202	58.12	168.62	21.858	0.844	0.133	0.181
203	126.83	169.31	22.382	0.272	0.211	0.248
204	49.02	169.45	20.277	1.046	0.039	0.053
205	308.46	172.22	21.537	1.120	0.092	0.211
206	110.17	174.09	21.461	2.121	0.071	0.228
207	27.93	175.14	21.958	0.280	0.122	0.173
208	141.73	176.04	20.989	0.886	0.052	0.091
209	43.68	177.92	22.067	0.325	0.183	0.210
210	148.83	178.27	20.919	0.075	0.057	0.065
211	110.46	180.22	21.018	0.474	0.083	0.112
212	92.99	180.99	20.521	1.191	0.037	0.065
213	12.16	180.92	21.221	1.369	0.079	0.150
214	139.77	181.54	20.523	1.075	0.056	0.085
215	41.69	181.78	21.423	0.902	0.113	0.159
216	112.39	182.81	20.642	1.420	0.055	0.103
217	121.57	184.91	21.622	0.421	0.083	0.120
218	94.05	185.12	22.377	-0.403	0.184	0.210

APPENDIX II (cont.)

ID	X	Y	V (mag)	B-V (mag)	σ_V (mag)	σ_{B-V} (mag)
219	81.37	188.47	21.878	1.129	0.108	0.227
220	44.41	191.39	21.013	1.226	0.062	0.110
221	61.09	194.95	22.450	0.030	0.198	0.249
222	22.47	198.34	22.014	1.161	0.132	0.239
223	123.13	199.29	21.997	1.060	0.132	0.238
224	310.07	199.81	22.158	0.572	0.191	0.246
225	43.78	203.35	21.470	1.140	0.098	0.163
226	70.94	203.65	20.868	1.109	0.064	0.109
227	27.98	203.31	21.211	1.245	0.082	0.140
228	74.33	204.87	21.154	0.467	0.070	0.092
229	8.10	204.73	21.386	1.176	0.106	0.175
230	50.88	206.85	22.503	-0.120	0.202	0.238
231	129.99	207.73	20.140	1.897	0.042	0.089
232	118.43	207.11	22.141	0.348	0.153	0.201
233	69.89	207.50	20.972	1.234	0.082	0.162
234	3.55	208.18	21.786	0.888	0.153	0.213
235	66.27	207.95	21.133	1.006	0.079	0.123
236	31.94	208.89	21.319	1.009	0.072	0.149
237	133.04	209.06	20.536	0.946	0.052	0.082
238	63.35	209.78	21.991	0.641	0.135	0.187

APPENDIX II (cont.)

ID	X	Y	V (mag)	B-V (mag)	σ_V (mag)	σ_{B-V} (mag)
239	138.31	210.01	20.574	1.288	0.047	0.071
240	88.03	211.00	21.306	0.213	0.064	0.090
241	84.59	211.38	21.896	0.721	0.116	0.195
242	144.40	212.68	21.684	0.972	0.118	0.172
243	132.68	213.36	21.890	0.678	0.150	0.211
244	158.89	214.07	21.539	0.831	0.095	0.132
245	149.62	215.37	21.931	0.102	0.133	0.169
246	42.94	217.63	21.681	1.640	0.127	0.245
247	133.69	218.40	20.758	1.557	0.047	0.113
248	85.32	218.75	21.674	1.129	0.075	0.169
249	9.97	220.38	20.347	1.465	0.039	0.074
250	117.97	221.68	22.059	1.039	0.098	0.181
251	77.85	223.09	21.832	-0.245	0.087	0.103
252	18.45	228.86	22.017	0.583	0.098	0.171
253	145.03	229.71	20.665	1.231	0.040	0.100
254	8.35	233.00	21.326	0.780	0.073	0.114
255	133.83	233.46	21.158	1.661	0.095	0.184
256	66.41	240.43	20.395	1.442	0.041	0.072
257	143.36	242.01	21.585	0.369	0.095	0.136
258	119.84	242.78	21.473	0.912	0.082	0.140

APPENDIX II (cont.)

ID	X	Y	V (mag)	B-V (mag)	σ_V (mag)	σ_{B-V} (mag)
259	175.00	243.93	20.635	1.569	0.042	0.248
260	155.73	243.82	21.151	0.627	0.070	0.113
261	169.74	244.49	21.507	1.009	0.096	0.164
262	280.13	248.64	21.852	0.678	0.154	0.203
263	165.10	250.42	21.354	2.068	0.064	0.239
264	76.51	250.36	20.299	1.160	0.036	0.057
265	136.92	252.05	21.155	1.131	0.071	0.190
266	121.97	251.98	21.970	0.711	0.126	0.212
267	167.95	253.73	20.846	1.727	0.061	0.154
268	86.95	253.77	21.629	1.056	0.113	0.159
269	175.61	255.97	19.905	0.888	0.029	0.048
270	117.73	257.17	21.201	1.348	0.081	0.145
271	41.48	256.81	21.874	0.960	0.116	0.204
272	309.58	257.22	20.461	1.564	0.036	0.076
273	128.93	258.51	21.246	1.265	0.056	0.115
274	22.71	260.07	22.229	0.258	0.165	0.220
275	102.33	261.36	21.991	0.553	0.101	0.177
276	111.89	261.58	22.325	0.743	0.144	0.243
277	194.45	263.20	21.779	0.608	0.108	0.150
278	201.84	262.87	21.707	0.235	0.089	0.122

APPENDIX II (cont.)

ID	X	Y	V (mag)	B-V (mag)	σ_V (mag)	σ_{B-V} (mag)
279	67.80	263.26	22.185	0.506	0.109	0.187
280	34.97	263.46	20.844	1.036	0.056	0.075
281	181.91	264.07	20.870	0.021	0.085	0.109
282	120.73	264.35	22.057	0.546	0.168	0.229
283	51.85	265.56	21.210	1.012	0.100	0.138
284	109.29	266.07	20.322	1.046	0.035	0.065
285	171.82	265.98	20.314	1.492	0.043	0.074
286	61.18	269.02	22.232	0.165	0.198	0.227
287	104.73	270.56	20.505	1.296	0.116	0.218
288	48.31	271.09	21.776	0.867	0.088	0.146
289	151.84	270.78	21.898	0.959	0.094	0.234
290	186.50	270.81	18.828	1.624	0.046	0.093
291	148.12	271.24	22.231	0.464	0.174	0.245
292	122.86	272.01	20.609	0.979	0.064	0.092
293	32.89	272.07	22.360	0.536	0.157	0.228
294	174.02	272.63	21.182	0.811	0.078	0.117
295	43.22	274.01	22.523	0.215	0.172	0.237
296	308.11	273.74	22.351	0.561	0.117	0.201
297	81.01	274.56	20.499	1.161	0.045	0.075
298	167.85	275.19	19.723	1.945	0.023	0.061

APPENDIX II (cont.)

ID	X	Y	V (mag)	B-V (mag)	σ_V (mag)	σ_{B-V} (mag)
299	24.46	275.41	22.180	0.821	0.127	0.197
300	198.22	277.07	21.956	0.572	0.138	0.197
301	89.87	277.20	21.101	0.636	0.091	0.129
302	28.69	277.84	21.758	0.770	0.112	0.163
303	220.09	278.22	20.848	0.808	0.108	0.140
304	113.65	278.30	20.392	1.480	0.044	0.135
305	159.78	279.84	22.110	0.218	0.140	0.171
306	151.70	279.53	21.085	1.155	0.052	0.100
307	125.40	280.33	20.210	1.420	0.050	0.077
308	165.59	280.78	21.607	-0.080	0.079	0.109
309	204.77	280.21	21.820	0.770	0.120	0.174
310	200.29	281.52	21.937	0.767	0.102	0.157
311	127.83	282.76	20.419	1.608	0.044	0.075
312	180.13	283.14	21.944	0.767	0.106	0.182
313	89.38	283.32	20.983	0.861	0.050	0.093
314	155.12	283.59	21.517	0.777	0.111	0.161
315	302.58	285.48	22.003	0.553	0.146	0.175
316	34.12	285.80	20.772	1.065	0.042	0.075
317	174.42	286.10	22.255	0.481	0.191	0.249
318	289.32	286.56	21.344	0.817	0.090	0.118

APPENDIX II (cont.)

ID	X	Y	V (mag)	B-V (mag)	σ_V (mag)	σ_{B-V} (mag)
319	112.22	286.74	21.227	1.289	0.068	0.158
320	229.16	288.99	21.812	0.594	0.096	0.148
321	193.07	288.77	22.349	0.682	0.152	0.224
322	85.71	289.29	21.452	0.164	0.068	0.089
323	45.55	289.98	21.752	0.663	0.097	0.147
324	275.47	290.23	22.066	0.527	0.122	0.187
325	162.06	291.84	22.042	0.537	0.139	0.235
326	104.88	294.03	21.809	0.735	0.118	0.169
327	14.76	293.92	21.249	1.246	0.067	0.153
328	205.54	294.87	22.276	0.240	0.152	0.229
329	97.38	294.56	21.081	1.137	0.048	0.109
330	166.73	295.25	22.123	0.474	0.104	0.169
331	226.82	295.40	21.169	1.260	0.085	0.137
332	215.08	295.78	21.811	0.893	0.099	0.164
333	209.93	296.17	22.089	0.086	0.132	0.187
334	202.53	295.85	21.692	0.746	0.112	0.217
335	263.83	295.83	20.921	1.772	0.031	0.136
336	302.79	295.73	21.011	1.196	0.063	0.160
337	112.00	296.61	20.889	0.990	0.051	0.097
338	23.75	296.97	22.394	0.524	0.158	0.223

APPENDIX II (cont.)

ID	X	Y	V (mag)	B-V (mag)	σ_V (mag)	σ_{B-V} (mag)
339	57.36	297.21	21.902	0.937	0.109	0.186
340	293.36	297.34	22.170	0.081	0.128	0.163
341	144.94	297.77	21.615	1.056	0.086	0.164
342	96.12	299.65	21.394	0.871	0.090	0.134
343	256.20	300.01	22.101	0.245	0.140	0.184
344	179.34	301.02	21.081	1.290	0.103	0.162
345	141.50	301.28	21.501	1.010	0.084	0.183
346	10.32	301.20	21.753	0.703	0.108	0.153
347	226.65	301.42	22.250	0.627	0.135	0.210
348	184.08	301.48	21.338	0.820	0.074	0.105
349	147.65	301.62	21.086	1.399	0.051	0.128
350	317.26	302.07	20.283	1.281	0.074	0.130
351	279.75	302.12	21.768	1.085	0.121	0.191
352	247.50	302.74	20.477	1.468	0.035	0.082
353	117.40	304.20	22.100	0.191	0.129	0.158
354	32.54	303.60	22.035	0.672	0.108	0.203
355	141.42	304.22	21.281	-0.049	0.117	0.137
356	110.84	304.68	20.210	1.296	0.022	0.056
357	239.36	305.19	21.493	1.045	0.096	0.136
358	172.87	306.84	20.662	1.283	0.043	0.086

APPENDIX II (cont.)

ID	X	Y	V (mag)	B-V (mag)	σ_V (mag)	σ_{B-V} (mag)
359	198.06	306.77	22.077	0.237	0.150	0.211
360	161.76	309.48	21.766	0.965	0.153	0.214
361	226.10	310.20	21.087	1.001	0.059	0.107
362	165.36	311.04	20.624	1.295	0.036	0.069
363	210.60	312.81	21.870	1.150	0.144	0.220
364	184.53	311.81	21.095	0.193	0.053	0.077
365	256.56	312.73	21.850	0.950	0.085	0.154
366	154.56	313.77	21.811	0.546	0.111	0.153
367	67.62	314.58	20.423	1.503	0.050	0.078
368	111.10	315.35	20.050	1.274	0.028	0.054
369	46.86	315.82	20.884	1.006	0.064	0.106
370	242.12	316.19	20.482	1.321	0.044	0.092
371	210.13	316.84	20.855	1.092	0.045	0.096
372	9.41	316.99	21.620	0.885	0.092	0.148
373	233.74	316.94	21.810	0.273	0.106	0.140
374	177.49	317.96	21.765	0.368	0.132	0.164
375	314.14	318.83	22.063	0.976	0.113	0.207
376	148.23	319.91	21.134	1.095	0.058	0.123
377	222.40	320.82	21.603	0.875	0.105	0.153
378	6.38	321.07	21.807	0.494	0.103	0.152

APPENDIX II (cont.)

ID	X	Y	V (mag)	B-V (mag)	σ_V (mag)	σ_{B-V} (mag)
379	127.02	321.71	22.017	-0.225	0.125	0.141
380	72.98	322.83	21.331	0.805	0.067	0.098
381	213.05	323.26	21.433	0.636	0.071	0.119
382	256.47	324.02	21.843	0.800	0.144	0.225
383	249.23	324.31	19.914	1.425	0.060	0.095
384	265.15	324.34	21.632	0.678	0.116	0.176
385	206.01	325.16	20.217	1.468	0.040	0.066
386	217.41	325.61	20.753	1.106	0.052	0.080
387	41.17	325.47	21.684	1.479	0.104	0.232
388	309.58	326.37	21.885	0.815	0.113	0.211
389	221.36	327.21	20.920	0.732	0.056	0.071
390	265.34	329.96	21.127	1.442	0.083	0.164
391	74.58	329.51	21.537	0.901	0.068	0.142
392	170.61	331.29	21.837	0.959	0.093	0.192
393	112.40	332.69	21.168	0.450	0.169	0.193
394	39.22	333.19	20.983	1.003	0.051	0.116
395	48.62	332.92	20.107	1.079	0.080	0.088
396	93.54	334.08	21.420	1.123	0.101	0.220
397	233.86	333.76	21.576	0.630	0.132	0.187
398	23.57	334.38	21.062	1.419	0.047	0.122

APPENDIX II (cont.)

ID	X	Y	V (mag)	B-V (mag)	σ_V (mag)	σ_{B-V} (mag)
399	236.01	335.96	21.155	1.065	0.095	0.151
400	108.30	335.82	21.722	0.338	0.087	0.137
401	162.33	335.65	22.045	0.788	0.151	0.195
402	285.83	335.97	21.501	0.608	0.223	0.237
403	151.52	337.54	21.859	0.792	0.162	0.212
404	141.10	337.45	22.421	0.581	0.170	0.237
405	72.15	338.87	22.383	0.263	0.163	0.199
406	54.33	339.22	22.090	1.091	0.106	0.222
407	22.55	339.53	21.975	0.528	0.132	0.169
408	262.57	340.14	21.408	0.957	0.086	0.122
409	160.64	341.39	22.304	0.397	0.138	0.208
410	29.24	342.71	20.766	1.160	0.073	0.106
411	205.30	343.09	21.801	1.336	0.110	0.215
412	243.40	342.97	21.878	0.943	0.122	0.166
413	97.10	343.21	21.076	0.964	0.059	0.138
414	197.73	344.53	21.511	1.573	0.069	0.178
415	217.78	344.18	21.120	1.368	0.058	0.149
416	204.43	347.28	20.178	1.971	0.032	0.084
417	189.97	347.35	22.074	0.896	0.128	0.209
418	50.60	347.69	21.365	1.250	0.060	0.160

APPENDIX II (cont.)

ID	X	Y	V (mag)	B-V (mag)	σ_V (mag)	σ_{B-V} (mag)
419	110.87	348.30	21.265	0.501	0.054	0.082
420	303.37	348.36	21.365	1.034	0.071	0.164
421	117.57	348.78	21.086	0.841	0.054	0.086
422	248.38	348.90	22.010	1.012	0.115	0.212
423	182.37	349.88	21.407	0.753	0.075	0.120
424	137.17	350.80	21.205	1.241	0.049	0.137
425	264.82	351.89	22.278	0.252	0.176	0.209
426	189.82	352.33	21.354	1.489	0.064	0.198
427	198.95	353.02	22.363	0.825	0.167	0.241
428	239.87	353.46	20.882	1.095	0.042	0.084
429	259.53	354.08	20.672	1.569	0.041	0.104
430	208.26	354.45	21.919	0.638	0.100	0.161
431	202.26	355.42	21.377	1.194	0.069	0.132
432	114.09	355.14	21.734	0.410	0.115	0.139
433	312.46	356.43	21.883	0.791	0.131	0.212
434	35.91	356.79	21.806	0.786	0.108	0.181
435	15.97	357.60	22.277	0.844	0.164	0.238
436	40.89	357.95	21.601	0.860	0.107	0.220
437	209.14	360.07	21.387	0.962	0.076	0.146
438	185.37	361.71	21.962	0.678	0.104	0.159

APPENDIX II (cont.)

ID	X	Y	V (mag)	B-V (mag)	σ_V (mag)	σ_{B-V} (mag)
439	188.95	362.20	20.346	1.402	0.035	0.079
440	273.80	362.12	22.253	0.352	0.171	0.229
441	279.05	362.99	22.098	0.491	0.124	0.169
442	219.52	364.01	22.014	0.915	0.108	0.198
443	8.23	364.84	22.072	0.289	0.139	0.197
444	300.60	364.85	21.254	0.937	0.061	0.110
445	57.89	365.02	19.878	1.124	0.028	0.042
446	125.48	365.83	20.706	1.402	0.032	0.089
447	190.07	367.24	19.890	1.803	0.022	0.050
448	156.88	367.06	21.933	1.169	0.140	0.228
449	91.38	368.03	22.202	0.287	0.167	0.207
450	266.23	369.46	21.335	0.798	0.053	0.104
451	16.70	370.41	21.851	0.860	0.111	0.222
452	55.47	371.97	22.105	0.661	0.159	0.225
453	160.27	373.64	20.608	0.817	0.039	0.064
454	192.99	374.08	21.766	1.157	0.089	0.225
455	224.62	374.43	21.654	0.865	0.064	0.148
456	56.00	375.05	21.195	1.131	0.080	0.151
457	254.54	374.80	21.553	1.005	0.075	0.171
458	303.44	377.11	20.231	2.118	0.058	0.178

APPENDIX II (cont.)

ID	X	Y	V (mag)	B-V (mag)	σ_V (mag)	σ_{B-V} (mag)
459	192.73	378.57	21.378	1.069	0.056	0.170
460	120.10	379.54	21.294	0.919	0.068	0.112
461	305.21	379.96	21.167	0.937	0.062	0.104
462	252.53	381.10	22.414	0.676	0.146	0.243
463	45.56	382.02	21.761	1.215	0.114	0.224
464	266.44	382.04	21.431	0.990	0.087	0.144
465	121.67	382.61	22.063	0.977	0.126	0.237
466	236.24	383.02	22.054	0.299	0.105	0.152
467	214.89	384.01	22.045	1.001	0.127	0.239
468	89.53	384.15	21.989	1.076	0.094	0.203
469	25.68	385.12	21.492	1.005	0.067	0.129
470	164.97	387.51	20.785	1.050	0.050	0.085
471	192.15	388.11	20.362	1.405	0.041	0.075
472	84.22	389.12	21.804	1.188	0.092	0.207
473	281.84	389.02	21.591	0.742	0.112	0.183
474	248.59	389.82	20.493	1.350	0.036	0.075
475	166.58	389.64	21.388	0.841	0.099	0.140
476	106.82	392.00	19.842	1.310	0.023	0.045
477	209.70	392.15	20.177	1.244	0.024	0.065
478	224.25	392.26	20.785	0.952	0.055	0.081

APPENDIX II (cont.)

ID	X	Y	V (mag)	B-V (mag)	σ_V (mag)	σ_{B-V} (mag)
479	91.69	393.12	21.243	-0.083	0.078	0.097
480	242.02	393.61	21.215	1.044	0.056	0.103
481	188.95	395.88	21.695	0.845	0.083	0.152
482	115.17	396.04	22.068	0.811	0.128	0.206
483	297.24	396.74	21.029	0.975	0.053	0.079
484	122.02	399.09	21.538	1.281	0.087	0.165
485	42.67	400.12	21.866	0.473	0.106	0.151
486	151.13	400.61	21.199	0.893	0.073	0.116
487	221.09	401.49	22.498	0.246	0.165	0.237
488	7.15	402.15	19.700	1.269	0.046	0.064
489	171.18	403.33	21.122	1.025	0.084	0.129
490	37.08	402.98	22.275	0.272	0.135	0.181
491	310.29	403.72	21.732	0.950	0.085	0.130
492	159.89	403.84	22.359	0.604	0.135	0.207
493	73.22	404.59	21.255	1.462	0.064	0.137
494	184.86	404.98	20.636	1.308	0.042	0.075
495	106.67	405.61	20.563	1.379	0.043	0.069
496	132.42	408.35	20.897	1.345	0.059	0.108
497	216.32	412.95	21.121	1.185	0.060	0.127
498	115.98	414.05	21.300	1.126	0.067	0.134

APPENDIX II (cont.)

ID	X	Y	V (mag)	B-V (mag)	σ_V (mag)	σ_{B-V} (mag)
499	151.88	413.95	21.142	0.935	0.068	0.123
500	190.53	414.15	21.934	0.800	0.106	0.179
501	108.34	414.59	21.350	1.250	0.081	0.137
502	265.24	415.93	21.116	1.348	0.044	0.138
503	226.50	417.14	20.798	2.819	0.042	0.209
504	247.39	421.17	22.112	0.358	0.133	0.177
505	174.65	420.97	21.671	0.228	0.161	0.179
506	110.31	420.88	21.545	1.341	0.087	0.165
507	222.10	423.19	20.926	0.995	0.053	0.082
508	140.47	423.29	21.654	1.087	0.090	0.206
509	271.83	424.25	22.244	0.133	0.170	0.203
510	31.15	425.33	22.073	0.608	0.110	0.177
511	128.74	425.33	21.076	0.965	0.068	0.111
512	226.61	425.41	21.787	0.701	0.102	0.156
513	178.88	425.91	21.293	0.752	0.078	0.098
514	165.41	427.90	21.444	0.746	0.075	0.099
515	217.04	428.12	21.882	0.965	0.119	0.182
516	17.43	428.38	21.620	0.931	0.063	0.141
517	135.79	428.95	21.292	1.080	0.074	0.143
518	311.07	428.89	21.082	1.139	0.052	0.090

APPENDIX II (cont.)

ID	X	Y	V (mag)	B-V (mag)	σ_V (mag)	σ_{B-V} (mag)
519	63.84	430.56	21.780	0.596	0.121	0.166
520	111.30	431.06	21.446	0.815	0.084	0.144
521	194.32	431.20	21.632	0.997	0.075	0.146
522	115.18	431.69	22.297	0.733	0.133	0.217
523	145.69	431.70	20.050	1.512	0.028	0.056
524	185.45	432.44	21.877	0.836	0.092	0.151
525	108.67	432.78	21.994	0.701	0.172	0.234
526	259.61	433.42	21.672	0.728	0.133	0.202
527	76.72	433.16	22.118	0.688	0.107	0.192
528	126.65	434.17	20.832	1.111	0.049	0.090
529	217.49	434.54	21.875	0.867	0.102	0.172
530	181.01	434.62	21.231	1.155	0.060	0.131
531	17.51	435.26	20.603	1.397	0.044	0.083
532	230.06	436.81	22.533	0.111	0.170	0.210
533	217.36	438.13	21.511	1.058	0.080	0.155
534	104.61	439.17	22.487	0.536	0.170	0.231
535	51.63	440.82	20.403	1.248	0.029	0.069
536	154.17	441.21	21.437	1.049	0.072	0.118
537	208.08	441.56	21.355	0.788	0.073	0.145
538	90.95	443.13	21.764	1.024	0.119	0.212

APPENDIX II (cont.)

ID	X	Y	V (mag)	B-V (mag)	σ_V (mag)	σ_{B-V} (mag)
539	171.18	443.13	20.991	1.301	0.060	0.112
540	55.54	443.18	21.216	1.027	0.062	0.122
541	77.11	444.32	20.579	1.071	0.033	0.071
542	289.62	446.95	21.720	0.815	0.069	0.138
543	248.75	450.46	21.512	0.914	0.069	0.119
544	162.76	452.98	21.990	0.508	0.120	0.187
545	71.66	453.90	20.291	1.512	0.037	0.069
546	149.96	456.15	22.212	0.481	0.115	0.178
547	139.58	458.87	21.149	1.047	0.040	0.089
548	32.16	459.22	21.961	0.578	0.088	0.150
549	98.62	459.88	21.385	1.217	0.059	0.137
550	23.39	460.95	20.389	1.221	0.050	0.075
551	311.85	462.29	22.121	0.852	0.131	0.248
552	239.10	461.56	22.133	0.407	0.113	0.166
553	124.08	465.15	20.735	1.055	0.035	0.070
554	178.16	465.46	21.299	0.952	0.067	0.111
555	311.60	465.56	21.735	0.712	0.094	0.180
556	228.92	466.45	21.754	0.847	0.117	0.201
557	79.44	467.39	19.832	1.313	0.039	0.060
558	286.56	467.86	21.901	0.713	0.125	0.177

APPENDIX II (cont.)

ID	X	Y	V (mag)	B-V (mag)	σ_V (mag)	σ_{B-V} (mag)
559	204.15	473.01	20.822	1.494	0.048	0.088
560	12.82	475.85	20.991	1.260	0.060	0.128
561	163.13	475.77	21.616	1.323	0.079	0.160
562	205.64	476.72	19.871	0.382	0.021	0.028
563	93.33	476.68	21.279	0.748	0.050	0.088
564	279.28	480.53	21.656	1.156	0.081	0.205
565	284.29	480.47	20.996	1.173	0.083	0.120
566	184.52	481.66	22.277	0.562	0.145	0.193
567	238.66	483.06	22.133	0.646	0.136	0.214
568	64.32	483.55	20.743	1.300	0.048	0.082
569	57.15	486.92	20.298	1.375	0.036	0.067
570	266.56	486.63	21.781	0.742	0.084	0.128
571	173.45	501.33	20.484	1.309	0.036	0.062
572	146.81	501.74	21.927	0.630	0.109	0.168
573	291.52	502.25	22.086	1.275	0.129	0.243
574	185.30	503.13	21.679	0.750	0.133	0.159
575	78.07	504.65	20.304	1.387	0.047	0.068

VITA

Surname: FOX Given Names: Michael Franz

Place of Birth: Wegberg, W. Germany Date of Birth: 18 september 1964

Educational Institutions Attended, with Dates of Entering and Leaving:

UNIVERSITY OF NEWCASTLE UPON TYNE, ENGLAND 1982 to 1985

UNIVERSITY OF VICTORIA, CANADA 1985 to 1987

Degrees, Diplomas, Etc., Awarded, with Dates and Names of Institutions:

B.Sc. 1985 University of Newcastle upon Tyne, England

Honours and Awards:

Sir George William Todd Prize, 1983

Russell Hindmarsh Prize, 1985

University of Victoria Fellowships, 1985/86 and 1986/87

Publications:

The Giant Branch of Leo I, Astron. J., June 1987, Vol. 93, p. 1381.

PARTIAL COPYRIGHT LICENCE

I hereby grant the right to lend my thesis (the title of which is shown below) to users of the University of Victoria Library, and to make single copies only for such users or in response to a request from the Library of any other university, or similar institution, on its behalf or for one of its users. I further agree that permission for extensive copying of this thesis for scholarly purposes may be granted by me or by a member of the University designated by me. It is understood that copying or publication of this thesis for financial gain shall not be allowed without my written permission.

Title of Thesis:

The Giant Branch of Leo I

Author: [redacted]
(Signature)

MICHAEL FRANZ FOX
(Name in block letters)

20 July 1987
(Date)